The role of particle shape on the stress distribution in a sandpile

BY I. ZURIGUEL* AND T. MULLIN

Manchester Centre for Nonlinear Dynamics, University of Manchester, Oxford Road, Manchester M139PL, UK

The results of an experimental investigation into the counter-intuitive phenomenon that a local minimum in the normal stress profile is sometimes found under the apex of a sandpile are presented. Specifically, the effects of particle shape on the stress distribution are studied and it is shown that anisotropy of the particles significantly enhances the dip. This amplification is attributed to the mechanical stability induced by boundary alignment of the anisotropic particles. Circular, ellipsoidal and pear-shaped cylinders are used and the stress propagates principally towards the sides of the pile through primary stress chains. Secondary chains are also present and we propose that the relationship between the magnitudes of the ratio of primary to secondary chains is correlated with the size of the dip.

Keywords: sandpile; granular; stress; chain; anisotropy

1. Introduction

Granular materials are ubiquitous in nature and industrial processes and have been studied for more than a century both because of their practical importance and considerable scientific interest. In more recent years, the interesting and often counter-intuitive properties of granular materials have attracted the attention of physicists where its collective behaviour is treated as a branch of condensed matter. This approach is reviewed by Jaeger *et al.* (1996), de Gennes (1999), Duran (1999) and Aranson & Tsimring (2006). One of the conceptually simplest examples of a collection of granular matter is the humble sandpile which is sometimes referred to as the 'silo problem' by engineers (Zhong *et al.* 2001). Despite its apparent simplicity, a complete description of the force structure within the pile has yet to emerge as reviewed by Atman *et al.* (2005) and Luding (2005). The system has been the focus of a great deal of attention since experimental investigations of Jotaki & Moriyama (1979), Smid & Novosad (1981), Brockbank *et al.* (1997) and Atman *et al.* (2005) reveal that a minimum in the normal stress can be found under the apex of the pile. This result, known as the pressure dip, is not only counter-intuitive but also challenges the isotropic elastic and plastic models, such as that of Terzaghi (1943), which are used to describe

*Author and address for correspondence: Departamento de Física y Matemática Aplicada, Universidad de Navarra, Pamplona 31008, Spain (iker@fisica.unav.es).

99

the mechanical properties of granular solids. An extensive review of various approaches to modelling properties of granular media is given by Savage (1998).

Several models have been proposed in attempts to understand the structure of the force network within a granular pile. For example, in the so-called 'q-model' proposed by Liu *et al.* (1995) and Coppersmith *et al.* (1996), it is assumed that the granular bulk can be described in terms of regular lattices of grains which interact through random contacts. One prediction of this model which is in accord with observations is the exponential force distribution found in the granular bulk. On the other hand, the q-model is unable to reproduce the pressure dip as discussed by Howell *et al.* (1999) and Veje *et al.* (1999). An alternative approach is provided by the fixed principal axes or 'FPA' model of Bouchaud *et al.* (1995). This is in accord with the experimental observation that stress in granular media tends to propagate linearly with preferred orientations as argued by Wittmer *et al.* (1996), Cates *et al.* (1998) and Atman *et al.* (2005). The preferred orientation of the stress is proposed to result from avalanching during the construction of the pile. Specifically, surface avalanches induce tent-like distributions of stresses that are subsequently buried and thereby frozen into the structure as originally put forward by Edwards & Oakeshott (1989) in a simpler model.

Hence, it may be surmised that the construction history of any given pile will be important in establishing its stress distribution. Vanel *et al.* (1999) and Geng *et al.* (2001, 2003) performed an experimental investigation into this by building piles using two pouring methods. In the so-called 'localized source procedure', the grains are poured from a hopper with an outlet diameter much smaller than the final size of the pile. This produces a dip under the apex of the pile. The 'raining' or 'distributed procedure' consists of pouring the grains in a distributed way and, in this case, no dip is found.

Discrete element simulations have also been used in attempts to understand the stress distribution in sandpiles in a number of studies. Modern accounts can be found in Liffman *et al.* (1994, 2001), Hemmingsson *et al.* (1997), Luding (1997), Matuttis (1998), Matuttis *et al.* (2000), Goldenberg & Goldhirsch (2005) and Li *et al.* (2005) and references therein. Effects which have been taken in to account include particle segregation by Liffman *et al.* (2001), horizontal compressive forces by Liffman *et al.* (1994) and Hemmingsson *et al.* (1997) and inter-particle friction by Luding (1997), Goldenberg & Goldhirsch (2005) and Li *et al.* (2005). Moreover, some preliminary studies of the importance of particle shape have been reported by Matuttis (1998) and Matuttis *et al.* (2000). While dips have been produced in many of these investigations, quantitative comparison with observation has not been performed. Perhaps, more importantly, a consensus of opinion on the principal mechanism that gives rise to the dip has yet to emerge.

An important characteristic of granular materials is that forces are observed to propagate through individual particle contacts giving rise to well-defined paths which are called force chains by Dantu (1968) and Liu *et al.* (1995). The chains form a characteristic network within the bulk as described by Jaeger *et al.* (1996) and de Gennes (1999) and are responsible for carrying most of the weight of the material or any load which is applied to it. These effects are pertinent even at very small length scales as shown by Ostojic *et al.* (2006). Force chains have also

been proposed to be the key to understand the jamming and yielding in granular media described by O'Hern *et al.* (2001) and Corwin *et al.* (2005). Liu *et al.* (1995) show that the force network can be characterized by estimating the probability distribution of individual contact forces, $P(F)$. $P(F)$ grows for small forces, has a plateau close to the mean force and decays exponentially for large values. Recent studies by Ostojic *et al.* (2006) suggest that there is a scale invariance in the spatial structure of the force network. The majority of the studies of force chains have been on two-dimensional systems where visualization is relatively easy, but Zhou *et al.* (2006) have recently provided new evidence for their importance in three-dimensional systems.

The understanding of the basic physical principles behind the stress transmission in static granular solids is clearly important as it can be applied in a range of practical situations ranging from silos to road and dam construction as reviewed by Zhong *et al.* (2001) and Li *et al.* (2005). In most practical situations, particles are mainly non-spherical (sand, cement, sugar, plastic pellets, etc.) and, in many cases, their shape is anisotropic (wheat, rice, …). Despite this, many model investigations of the stress distribution in the canonical problem of a sandpile use circular or spherical particles. Huntley (1999) discusses this point and shows significant effects in experiments using a range of particles. The idealization of sphericity in simulations and experiments may give rise to non-generic features since the building blocks of the pile have special symmetries. Indeed, previous investigations of the behaviour of granular media in other configurations have shown important effects of particle shape. These include investigations of the particle packing fraction by Sugden (1980), Donev *et al.* (2004) and Lumay & Vandewalle (2004), wall pressures in the discharge of a silo by Nielsen (1998) and Zhong *et al.* (2001) and jamming in the flow of grains through an orifice by Zuriguel *et al.* (2005). The general consensus from all of these studies is that orientational effects of the particles are important.

Our thesis is that the effect of particle shape may play an influential role in the stress distribution under a sandpile. Here, we report the results of an experimental investigation into making specific changes to the shape of the particles used to construct the pile. Our experiments are all two dimensional and we use circular, elliptic and pear-shaped cylinders made from a photoelastic material to visualize the stress network in the pile in the manner first reported by Drescher & De Josselin de Jong (1972). The present investigation builds on a recent study by Zuriguel *et al.* (2007) where it is shown that using elliptical cylinders significantly enhances the stress dip. It is also shown that the primary and secondary stress chains have preferred angular orientations and the ratio of their magnitudes is correlated with the magnitude of the dip. We have also performed experiments using pear-shaped particles and carried out more extensive sets of analysis of the orientation of the particles, which indicate that mechanical stability is important in the creation of a dip under a sandpile.

2. Experimental method

A schematic of the experimental apparatus is presented in figure 1. It consisted of an aluminium frame, which was 157 cm wide and 100 cm high, mounted vertically on bearings in a stand so that it could be rotated about the horizontal axis. This
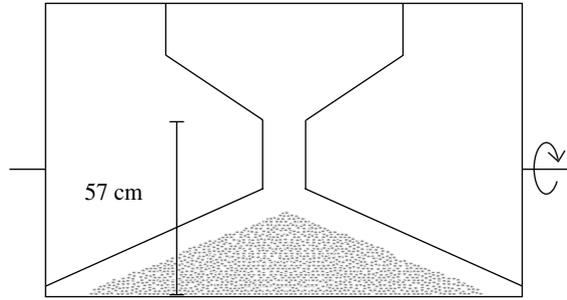
Figure 1. Sketch of the experimental set-up.

enabled the repeated construction of 500 piles in a reasonable amount of time, so that good statistical averages of the stress distributions could be obtained. The front and back of the apparatus were made from 10 mm thick pieces of Perspex sheet which were held 7 mm apart by the aluminium frame. These divided the apparatus into three regions as shown in figure 1. The test compartment, where the piles were built, was 35 cm high and had a flat bottom. The top compartment, which acted as a hopper where the particles were stored prior to discharge, has sloped walls set at 52° to the horizontal. Finally, a 22 cm long and 7 cm wide channel connected the hopper with the test compartment. The bottom boundary was made of both aluminium and hard rubber with no observable effect on the results. Piles were hence built in the so-called localized source procedure of Vanel *et al.* (1999) and Geng *et al.* (2001), as the grains were poured from the hopper outlet which was 7 cm wide and was located 57 cm above the base.

The experiments were essentially two dimensional since the particles were cut from 6.6 ± 0.1 mm thick sheets of photoelastic polymer material (Measurements Group, material PSM-4) using high-precision computer-controlled water jets. This enabled us to choose distinct shapes for the particles and we show examples of them in figure 2. The first set of particles investigated consisted of a mixture of 2500 discs with diameter 6.9 mm and 500 discs with diameter 8.9 mm where a selection of them are shown in figure 2*a*. The particle sizes were chosen to be the same as used in the previous investigations by Geng *et al.* (2001). The second set comprised 2900 elliptical cylinders with dimensions 9.9 and 4.9 mm on the major and minor axes as shown in figure 2*b*. The third sample consisted on 1900 pear-shaped cylinders with examples shown in figure 2*c*. The pear shape was defined by $y=\sqrt{tb^2(1-(x^2/a^2))}$, where $a=4.95$, $b=2.45$, $t=(1+kx)/(1-kx)$ and $k=0.13$. In all cases the polydispersity of the particles was less than 2%.

The average angle of repose found for 500 piles of discs was $27\pm1°$, $35\pm1°$ for elliptic cylinders and $40\pm2°$ for pear-shaped cylinders. The height and width of the piles were, respectively, 28 and 110 cm for discs, 31 and 88 cm for elliptic cylinders and 28 and 69 cm for pear-shaped cylinders. In all the cases, the packing fraction was 0.82 ± 0.01, which is just below the random close-packed limit of 0.84 in two dimensions (Xu *et al.* 2005).

The material used to make the particles is birefringent under strain, and this property may be used to obtain estimates of the stress distribution as shown by Howell *et al.* (1999), Veje *et al.* (1999) and Majmudar & Behringer (2005). The piles were back lit by a uniform sheet of light formed using an extended light
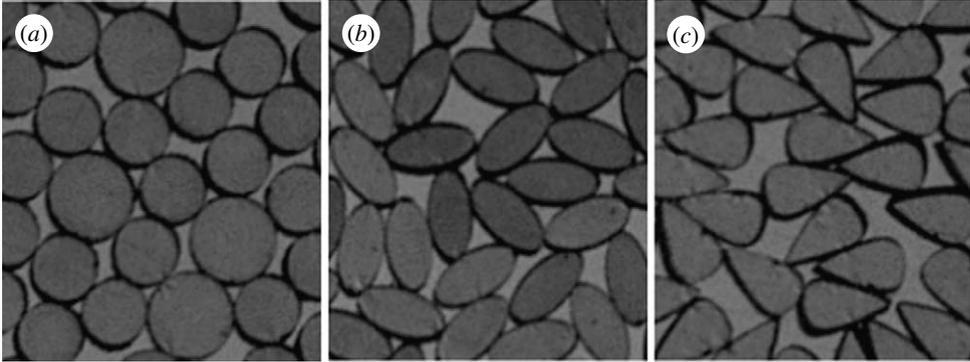
Figure 2. Image of the particles as they are arranged within the pile. (*a*) Mixture of discs, (*b*) elliptic cylinders and (*c*) pear-shaped cylinders.

source passed through a diffuser and viewed from the front through a pair of cross-polars. Two examples of piles are shown in figure 3 where typical chain structures can be seen. The one shown in figure 3*a* was constructed from the mixture of discs and the other in figure 3*b* using elliptic cylinders. A six megapixel Nikon digital camera was used to capture images of the stress field from a region which was 50 cm long and 33 cm high. The images were stored on an associated computer for further processing. The method used to estimate the stress distribution in the pile is based on the material property that a load on the particles produces bright fringes whose number increases in proportion to the force as discussed by Majmudar & Behringer (2005). Specifically, the square of the gradient of intensity of the transmitted light is proportional to the stress acting on the particle. The technique requires an independent calibration and this was done for each particle shape by applying 30 different known loads to a set of thin layers of grains held between solid boundaries which were 18.9 cm wide and 3.7 cm high, i.e. an aspect ratio of approximately 5 so that end-wall boundary effects were reduced. Every load was applied five times in order to obtain good statistical averages for each particle configuration. The average vertical stress over the whole layer was found to be proportional to $|\nabla I|^2$ using a third-order polynomial fit to the response data, where $|\nabla I|^2$ is calculated at the pixel scale. The regression coefficient of the fit was 0.99 in all cases. The resulting calibration curve for discs is given in figure 4 and very similar data were found for ellipses and pears. A minor limitation of the technique was that vertical stresses smaller than $0.5\,\mathrm{N\,m^{-1}}$ were not detected.

An advantage in using photoelastic particles was that the principal stress distribution was readily made visible and this enabled the analysis of the structural properties of the force network. As can be seen in figure 3 the force chain structure appears to be different in images for both the discs and the elliptic cylinders. The chain structure for discs seems to be more open and a complex pattern is evident in the case of elliptical cylinders. However, quantitative analysis is required before definite statements can be made concerning the apparent differences in chain structure.

In general, the stress network has a rich structure that makes detailed quantitative analysis difficult to perform. However, Zuriguel *et al.* (2007) have shown that the chains can usefully be considered as comprising short linear
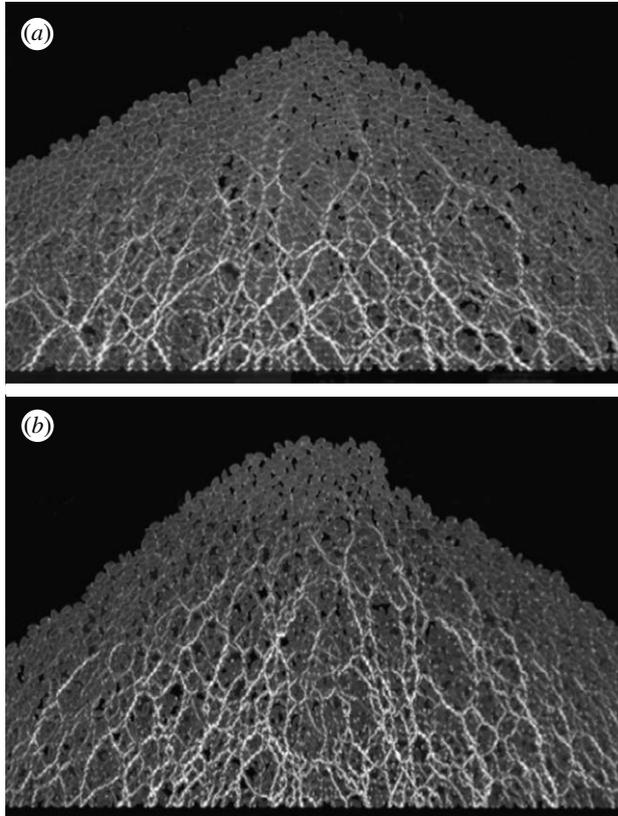
Figure 3. Example of piles of (*a*) discs and (*b*) elliptic cylinders viewed through the two cross polarizers. The stress chains can be clearly seen as bright lines in the images. The force networks seem to be different for discs and elliptic cylinders but statistical analysis of many repetitions of the experiment are required to uncover the properties of the stress chains.

segments which change direction at branch points. This observation enables the division of the entire chain network into smaller links where each section has a well-defined position, length and orientation. An important point to note is that while chains must pass from particle to particle through contacts, they do not necessarily go through the centres of the grains. This presumably reflects the importance of tangential forces which arise through particle friction.

The procedure to identify the chains was as follows. An intensity threshold was applied to convert the greyscale images to black and white format. Reflections from the edges of the particles, which produced spots of light smaller than 0.5 cm, were removed. The chains had a finite width where the value depended on the intensity threshold applied. Our interest lay in the orientation of the chains and hence we reduced all the chains to one-pixel wide lines by homogeneously eroding the edges. This reduction technique was checked for different intensity thresholds and we obtained consistent results over a range of threshold values. The whole network was divided into segments by identifying the branch points (figure 5). A linear least-squares fit procedure was performed on every line and hence estimates of the position, length and orientation of the chains were obtained. The orientation of the chains (ϕ) is defined as the angle that the identified stress chain made with the
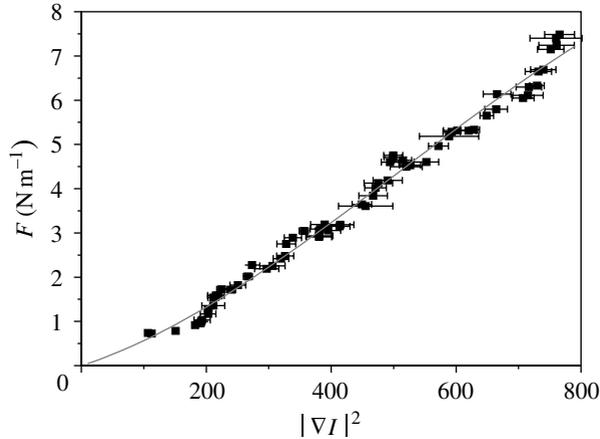
Figure 4. Monotonic increase of $|\nabla I|^2$ when different vertical stress is applied to a thin layer of discs. The error bars are the standard deviations of $|\nabla I|^2$ for the five measurements taken for each applied load. The solid line is a third-order polynomial fit $P = a(|\nabla I|^2) + b(|\nabla I|^2)^2 + c(|\nabla I|^2)^3$, where $a = 4.537 \times 10^{-3}$, $b = 1.197 \times 10^{-5}$ and $c = 7.793 \times 10^{-9}$.
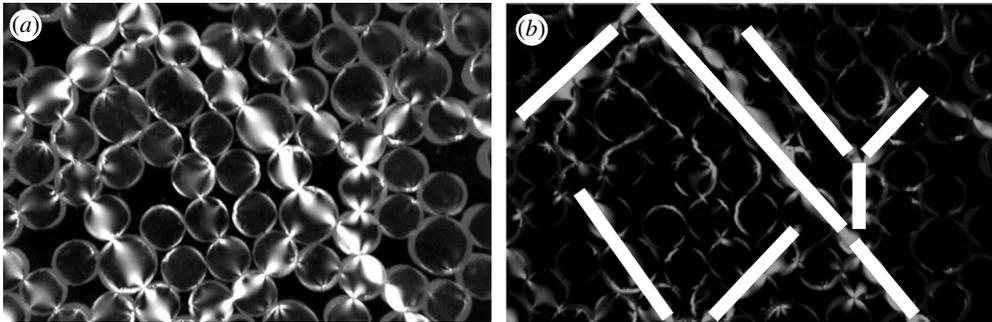
Figure 5. (*a*) Close-up image of the chains that build up the stress network. In (*b*) least-squares fits are shown.

normal to the base and was measured with an experimental error of approximately 2°. A typical number of chains obtained in a single pile was 200, and consequently 10^5 chains were obtained for 500 piles. The data reduction technique outlined above is in the spirit of the structure identification techniques proposed recently by Ostojic *et al.* (2006).

Another interesting measurement that can be made for the non-circular particles is the orientation of the particles within the pile. In order to obtain the estimates of the particle orientation, images of the piles were captured without the cross polarizers in place. A bespoke particle recognition program using routines from within the 'MATLAB' suite was used to obtain the position and orientation of every particle. The orientation of the elliptic cylinders (θ) is defined as the angle that the long axis of the ovals makes with the normal to the base. For the pear-shaped cylinders, the orientation is defined as the angle that the bisector of the particles makes with the normal to the base. Note that the orientation for elliptic cylinders ranges from $-90°$ to $+90°$ whereas for a pear-shaped cylinder it goes from $-180°$ to $+180°$.
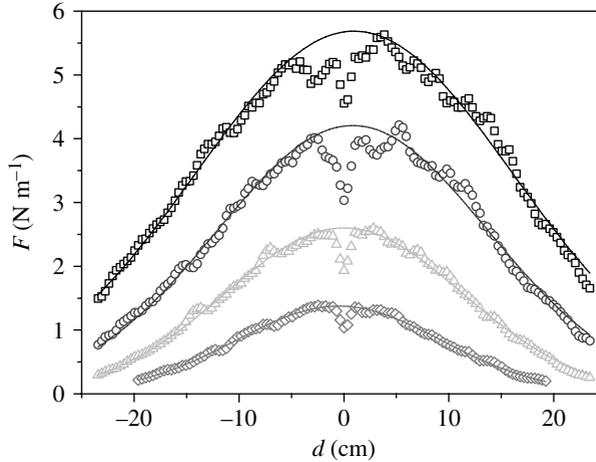
Figure 6. Vertical stress distributions estimated from averaging the results of 500 repetitions of piles built from a localized region with a mixture of 2500 discs with diameter 6.9 ± 0.1 mm and 500 discs with diameter 8.9 ± 0.1 mm. The stresses were measured at $h = 3.5$ cm (squares), $h = 7.0$ cm (circles), $h = 10.5$ cm (triangles) and $h = 14.0$ cm (diamonds) above the base.

3. Results

The first set of results shown in figure 6 are estimates of the average vertical stress profiles inside the pile at heights $h = 3.5$, 7.0, 10.5 and 14.0 cm above the base. These were obtained for piles of discs and a dip is visible at all heights. This result is in excellent agreement with those obtained by Geng *et al.* (2001). Furthermore, we have found that a Gaussian provides a good least-squares fit over most of the profiles except for the region of the dip. The fits are shown as solid lines in figure 6 where averages were taken over 500 pile constructions.[1]

Zuriguel *et al.* (2007) showed that the use of elliptic cylinders had a dramatic effect on the size of the dip when the grains were poured from a localized source. In order to quantify the size of the dip, we define F_D as the difference between the full experimental datasets and Gaussian fits to the profiles obtained using the respective particles. Hence, if there is a dip in the stress profile, F_D will display negative values near the centre of the pile as the actual vertical stress will be smaller than the value of the Gaussian fit. The values of F_D are displayed for piles of discs, elliptical cylinders and pear-shaped cylinders in figure 7*a–c*, respectively. For all cases, the curves represent the average stress difference from the Gaussian profile of 500 piles at $h = 3.5$, 7.0, 10.5 and 14.0 cm above the base.

This procedure can be used to make direct comparisons between the vertical stress profiles of piles constructed using discs, elliptical cylinders and pear-shaped cylinders (figure 7*a–c*, respectively). A dip is present in all results but the size of the dip is clearly largest for pear-shaped cylinders, slightly smaller for elliptical cylinders and greatly reduced for discs. Quantitative comparisons between the profiles measured at 3.5 cm above the base show that the amplitude of the dip is approximately four times larger for elliptical cylinders than for discs

---

[1] Data points within ± 7.5 cm of the centre of the profile were not used in the fitting procedure. It was established empirically that omitting data over this region produced robust results for all piles.
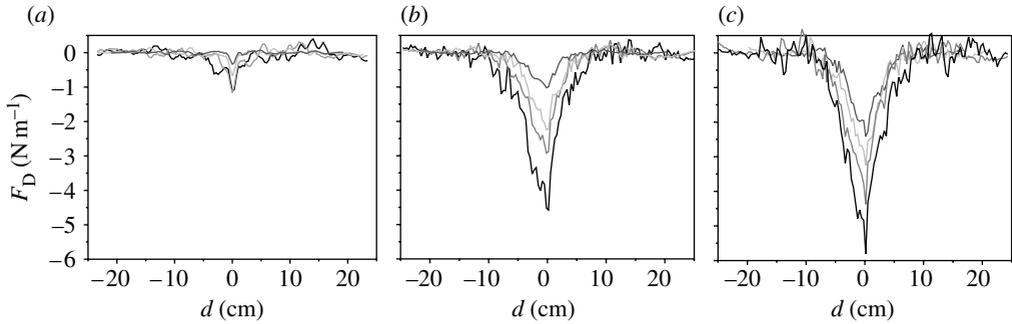
Figure 7. Difference between the vertical stress profiles measured experimentally and the Gaussian fits for (*a*) discs, (*b*) elliptic cylinders and (*c*) pear-shaped cylinders when they are poured from a localized region at 57 cm. The different lines represent—from bottom to top—the stress differences calculated at $h = 3.5$, 7.0, 10.5 and 14.0 cm above the base. Note that (*a*) is just the difference between the experimental data and the fit shown in figure 6.

and approximately five times larger for pear-shaped cylinders than for discs. Integrating the area under the F_D curves, we find that the dip is approximately 6.5 times bigger for elliptic cylinders than it is for discs. The effect is increased for pear-shaped cylinders where it is approximately 7.5 times bigger than for discs. These results confirm the observations of Zuriguel *et al.* (2007) that the shape of the particles has an important effect on the vertical stress profile of sandpiles as the dip is enhanced by the anisotropy of the grains.

Properties of the stress chains were analysed in an attempt to shed light on the origin of the dip in sandpiles. The first property examined was the distribution of the lengths of chains (l) in centimetres. The chain length distribution calculated for 500 piles for each particle shape was found to be exponentially distributed for all piles. The results for elliptic cylinders are presented in figure 8 and those for discs and pears had qualitatively similar characteristics. They are all in accord with the force distribution in granular solids found by Liu *et al.* (1995). The characteristic length of the exponential distribution (l_c) depended on the particle shape as follows: $l_c = 0.690$ cm for discs; $l_c = 0.584$ cm for elliptic cylinders and $l_c = 0.609$ cm for pear-shaped cylinders. These results suggest that chains in piles of discs were slightly longer than for other particle shapes. This 15% difference in the characteristic length is consistent with the more open chain structure for discs visible in figure 3*a*. A more complex pattern is visible for elliptic (figure 3*b*) and pear-shaped cylinders (not shown) since there are more chains with a smaller value for the characteristic length.

The images of the piles presented in figure 3 suggest that chains have preferred orientations and this feature was quantified by the estimated probability distribution of chain orientations over the whole pile. There are distinct peaks at $\pm 35°$ displayed in the distribution shown as an inset of figure 9. This observation is in accord with the fact that the contact distribution for piles of discs displays peaks at $\pm 30°$ which is in very good agreement with a previous work of Geng *et al.* (2001). The close correlation between the orientation of force chains and contacts is expected since the chains pass from particle to particle through contacts. However, they do not necessarily go through the centres of the grains, which are presumably an effect of tangential forces resulting from inter-particle friction.
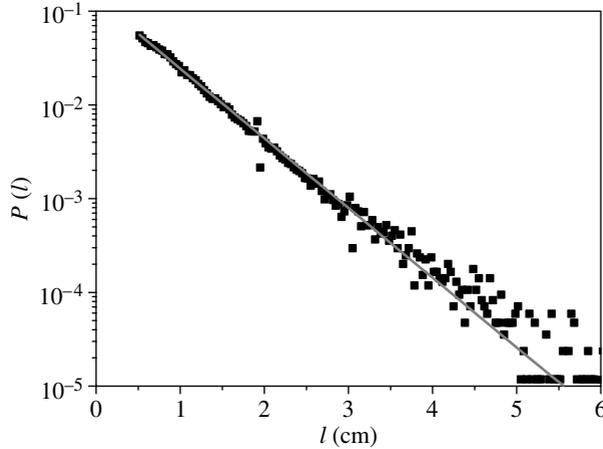
Figure 8. Semilogarithmic plot of the chain length distribution for the mixture of elliptic cylinders. The experimental data are fitted with an exponential function $P(l) = A\mathrm{e}^{-l/l_\mathrm{c}}$ where $A = 0.135$ and the characteristic length $l_\mathrm{c} = 0.584$.

In order to obtain further insight into the geometry of the chain network, measures were taken in thin slices across the pile. It seemed logical to take slices aligned with the angle of repose of the pile but this did not reveal any interesting results and the chain orientation within different slices all appeared similar. A more interesting result became apparent when the probability distribution of the orientations of chains was measured for different thin (1.5 cm thick) vertical slices along the '*x*'-direction of the pile as indicated in figure 9. There were between 30 and 33 slices taken across each pile where the exact number varied between experiments. Our *a posteriori* justification for this approach is the following. The distance a particle travels after it has impacted with the apex of the pile until it comes to rest is proportional to the distance from the centre of the pile. Hence any structure which is frozen into will be correlated with the distance from the centre. This assumption is valid if the angle of repose remains approximately constant as the pile grows.

Histograms of the orientations of chains within different vertical slices of 1.5 cm width are presented in figure 9. The distributions are for piles constructed using discs and contain two peaks at $\pm35°$. The amplitudes of the peaks for each distribution are generally different and they are only the same for the central slice.

The following bimodal distribution function was chosen to fit the data:

$$P(\phi) = cf(\phi; +35, \sigma_1) + (1-c)f(\phi; -35, \sigma_2),\qquad(3.1)$$

where c is a constant ($0 \le c \le 1$); f are normal distribution functions with centres at $\pm35°$; and the corresponding standard deviations are σ_1 and σ_2. Note that the values of c and $1-c$ indicate the relative area under the normal distributions centred at $+35°$ and $-35°$, respectively.

A result which is clear in figure 9 is that the chain orientation distribution depends on the distance to the centre of the pile (d). Generally, the peak at $+35°$ is bigger than the peak at $-35°$ for regions on the r.h.s. of the pile ($d>0$) and
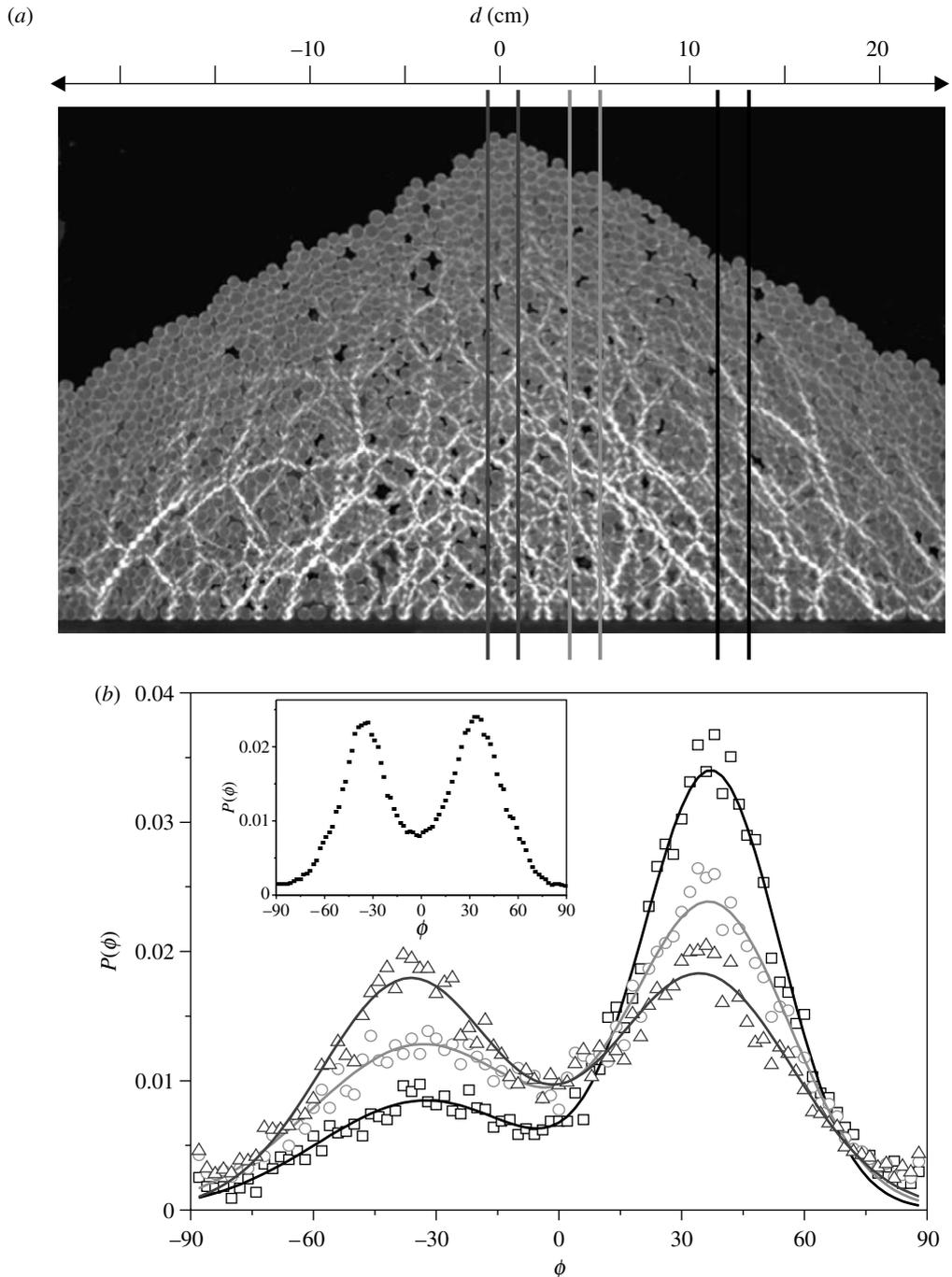
Figure 9. (*a*) Typical vertical slices used in processing chain orientation. (*b*) Bimodal distribution obtained for the orientation of the chains along the '*x*'-direction of the pile. Squares, circles and triangles represent the orientations for the chains that fall in vertical slices of 1.5 cm width centred at *d*=12.0, 4.5 and 0 cm, respectively. The solid lines are the correspondent fits with equation (3.1). (Inset) Orientation probability distribution of chains over the whole pile. The results are for piles of discs built from a localized source and similar curves are obtained for other particle shapes.
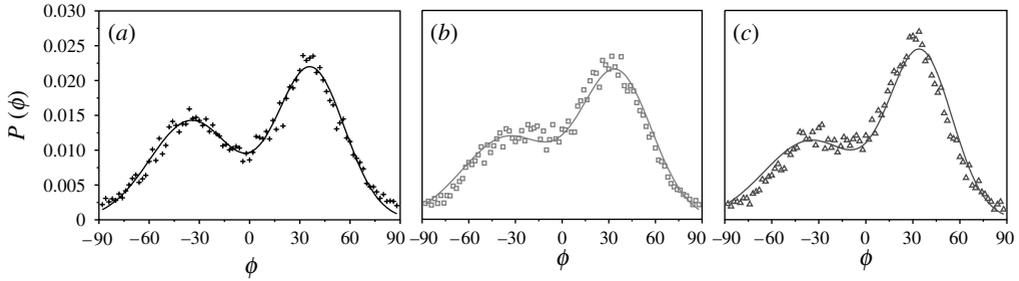
Figure 10. Probability distributions for the chain orientations calculated from 500 piles in a 1.5 cm slice located at $d=3.0$ cm from the centre of the pile: (*a*) discs, (*b*) elliptic cylinders and (*c*) pear-shaped cylinders. The ratios between the amplitude of the main and secondary peaks are: discs, 1.53; elliptical cylinders, 1.81; pear-shaped cylinders, 2.15.

vice versa for the l.h.s. Hence, the primary chains on the r.h.s. of the pile tend to be oriented towards the right with the mirror image on the left. The distribution of the orientations of the chains, which lie in the central region of the pile ($d=0$), has two peaks of equal size so that there is a continuous transition between the l.h.s. and r.h.s. The bimodal nature of distributions of the chain orientations at all 'x' positions across the pile indicates the presence of primary and secondary chains at $\pm 35°$ where the small peak corresponds to secondary chains perpendicular to the primaries. The results presented in figure 9 illustrate that the number of secondary chains decreases with the distance from the centre of the pile.

Qualitatively similar results were obtained for elliptical and pear-shaped cylinders with the main difference being the magnitude of the peaks at $\pm 35°$. This is illustrated by the results presented in figure 10 where probability distributions for the chain orientations calculated from slices located $d=3.0$ cm from the centre of the pile. A clear feature of these distributions is the relative magnitude of the peaks and this can be evaluated by estimating the area under the two normal distributions for different d, i.e. representing the value of the constant c in equation (3.1) for different d. An alternative method is to calculate the average orientation of the chains ($\langle \phi \rangle$) and its dependence on d. Both analyses produce similar results but the error obtained using the average orientation of the chains is much smaller since $\langle \phi \rangle$ is obtained directly from the raw data whereas c is obtained from a fit. Hence the latter method was used.

The results of the dependence of the average orientation ($\langle \phi \rangle$) of the chains on the distance to the centre of the pile (d) are presented in figure 11 for piles of discs (circles), elliptic cylinders (triangles) and pear-shaped cylinders (diamonds). We observe that in all the cases, the average orientation is vertical ($0°$) in the centre of the pile. This is consistent with the finding that the two peaks of the bimodal distribution have approximately the same size at $d=0$ as shown by the data with the triangles in figure 9. For the regions of the pile far from the centre, there is only a weak dependence of ϕ on the shape of the grains. Indeed in all the cases the average orientation tends to be $+35°$ in the right end and $-35°$ in the left end of the pile. Note that by left or right end of the pile we mean the limit of the region of the pile analysed, i.e. $d=\pm 25$ cm (figure 3).
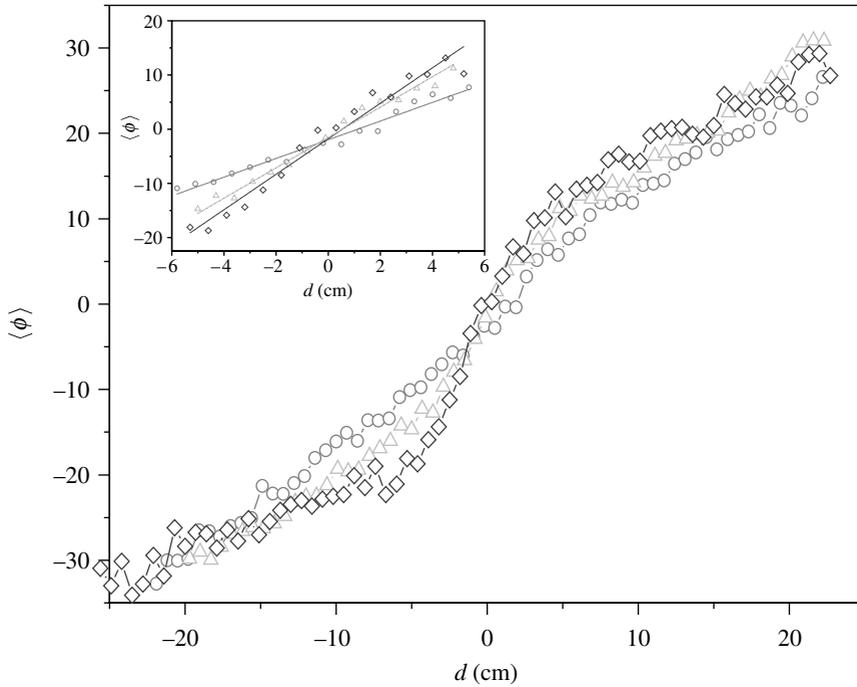
Figure 11. Mean chain orientation for different positions along the x-direction of the pile. Circles, triangles and diamonds represent $\langle\phi\rangle$ for discs, elliptic cylinders and pear-shaped cylinders, respectively, poured from a localized region at 57 cm. The inset contains a close-up of the data for the central region of the pile. Solid lines are linear fits of the data with slopes: $1.7^\circ\,\mathrm{cm}^{-1}$ for discs, $2.8^\circ\,\mathrm{cm}^{-1}$ for elliptic cylinders and $3.2^\circ\,\mathrm{cm}^{-1}$ for pear-shaped cylinders.

The main difference between the chain orientations for different particle shapes is revealed in the central region of the pile as shown in the inset of figure 11. For piles of discs, the slope of the linear fit to the variation of the mean angle of the chains along the x-direction is found to be $1.7^\circ\,\mathrm{cm}^{-1}$. For the piles of elliptical cylinders, a more rapid transition is obtained with a slope of $2.8^\circ\,\mathrm{cm}^{-1}$. Hence, near the centre of the pile, the secondary chains are of lesser importance for elliptical cylinders than discs. This transition from negative to positive values of $\langle\phi\rangle$ is even sharper for pear-shaped particles at $3.2^\circ\,\mathrm{cm}^{-1}$. Consequently, we conclude that there is a correlation between the slope of $\langle\phi\rangle$ versus d in the centre of the pile and the size of the dip in the vertical stress profiles.

The principal feature which distinguishes between isotropic and anisotropic particles is the ability of the latter to adopt different spatial orientations. An investigation of the orientation of individual particles in the pile provided further insight into the way the particle shape affected the size of the dip. The distribution of the orientations of the elliptic cylinders averaged over 500 piles is presented in figure 12. The orientation of the elliptic cylinders (θ) is defined as the angle that their long axes make with the normal to the base. It can be seen in figure 12a, where the distribution is averaged over the whole pile, that the particles are mainly oriented horizontally. Hence, the particles adopt the optimally stable orientation for an ellipse on a horizontal surface and this ordering by the base is maintained vertically through the pile, i.e. orientation by avalanching is weak. Indeed, the orientation probability is
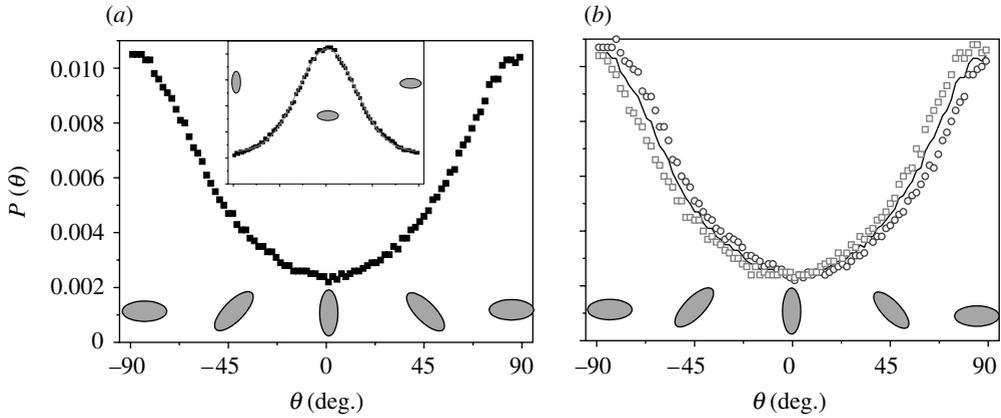
Figure 12. Orientation of the elliptic cylinders in the pile. (*a*) Probability distribution of all the elliptic cylinders in the pile. In the inset, the particle orientations are plotted with respect to the horizontal and a Gaussian distribution centred about zero is clear. (*b*) Probability distribution of the elliptic cylinders in the right of pile (squares) and in the left of the pile (circles). The solid line represents the probability orientation over the whole pile.
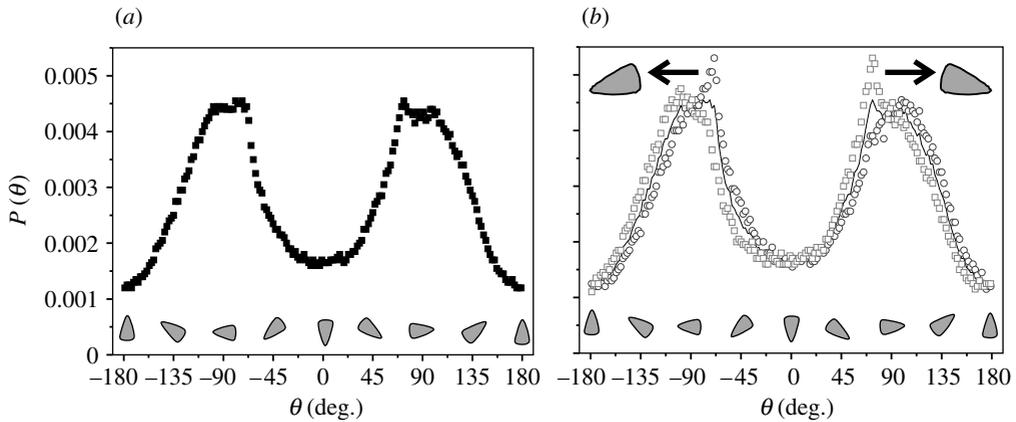
Figure 13. Orientation of the pear-shaped cylinders in the pile. (*a*) Probability distribution of all the pear-shaped cylinders in the pile. (*b*) Probability distribution of the pear-shaped cylinders in the right of pile (squares) and in the left of the pile (circles). The solid line represents the probability orientation over the whole pile.

a normal distribution with a maximum probability for the horizontal orientation as shown in the inset of figure 12*a*. This result is in accord with numerical simulations of packing of ellipses by Buchalter & Bradley (1992) and Nouguier-Lehonn *et al.* (2003) and experiments and simulations of the orientation of prolate granular materials (Stokely *et al.* 2003).

It is well known that under certain conditions anisotropic grains tend to be aligned with the flow direction as discussed by Lumay & Vandewalle (2004). In order to investigate this possibility, the particle orientation distribution was analysed independently for both sides of the pile. Specifically, flow alignment would produce a peak at the angle of repose. For the case of elliptical cylinders, these peaks should be at $+55°$ and $-55°$ for the r.h.s. and l.h.s. of the pile,

respectively, i.e. $90 - \alpha_{rep}$ where $\alpha_{rep} \approx 35°$ here. The angular distributions for elliptic cylinders are shown in figure 12*b* for the l.h.s. and r.h.s. of the pile and there are no obvious peaks at $\pm 55°$. There is a small dependence of the particle orientation on location since the orientations with positive values ($\theta > 0$) are more likely to be found on the r.h.s. and vice versa for ($\theta < 0$). Thus, there is a weak orientation of the particles with the direction of the flow, i.e. parallel to the surface. These results reaffirm the findings obtained using the global average that the flow plays a minor role in orienting the particles and the preferred orientation of the particles is horizontal.

Qualitatively similar results were obtained for the orientation of pear-shaped cylinders as shown in figure 13*a* where we note that these particles can be oriented over the full 360°. The orientation probability distributions contain equal size peaks which correspond to horizontal orientation to the left or right. Thus, as in the case of elliptic cylinders, the preferred orientation is horizontal but now there is a distinction between left and right. Interestingly, the probability that a pear-shaped cylinder points downward ($\theta = 0$) is higher than upwards ($\theta = \pm 180$). The orientation distribution formed separately for the l.h.s. and r.h.s. of the pile is shown figure 13*b* and it is also in accord with the orientation distribution of elliptical particles. All the orientations with $-180 < \theta < -90$ and $0 < \theta < 90$ are more likely on the r.h.s. of the pile than on the left. Equally, all orientations with $-90 < \theta < 0$ and $90 < \theta < 180$ are more likely on the l.h.s. of the pile than on the right. Hence there is weak orientation of the particles by the flow since there is a small preference of the particles to be aligned parallel to the surface of the pile.

In-depth analysis of the orientation distributions for elliptical and pear-shaped cylinders for the r.h.s. and l.h.s. of the pile reveals an important difference between the two sets of results. The distributions are symmetric for elliptical cylinders whereas these are asymmetric for pear-shaped cylinders. Moreover, the maximum orientation probability for pear-shaped cylinders on both r.h.s. and l.h.s. of the pile is found at $\theta = 70$ and -70, respectively. These values are in accord with the most stable orientation of a single pear-shaped cylinder on a horizontal surface which is $\theta = \pm 70$. A schematic of this orientation is given in figure 13*b* where it is indicated by arrows.

4. Conclusions

We have demonstrated that the presence of a dip in the vertical stress profile of a sandpile is robust for a range of particle shapes when the grains are poured from a localized source. Particle shape plays an important role on the stress transmission within the pile since introducing an anisotropy into the particle shape magnifies the dip considerably. Analysis of the angular distribution of the force chains has provided insights into the stress transmission within the pile. The distributions have significant peaks at $\pm 35°$ which correspond to the orientation of the primary chains with minor peaks in orthogonal directions for the secondary chains. Hence the primary force chains are mainly structured in the way described by Edwards & Oakeshott (1989) and Cates *et al.* (1998), but secondary stabilizing chains are also present. These presumably arise from frictional effects and are not encompassed within the models.

Our principal finding is that there is a direct correlation between the size of the dip and the mean chain orientation within the pile. Our interpretation of this result is that if all the load is carried towards the sides of the pile by primary chains in a tent-like structure, the dip in the vertical stress profile under the centre of the pile would be very large because of the sudden switch in the mean chain orientation at $d=0$. However, the presence of secondary chains, which carry the load of the pile towards the centre of the pile, mediates this changeover and hence reduces the size of the dip. It is our thesis that the secondary chains are essential ingredients in the mechanical stability of the pile. The number of secondary chains is greater for discs than for either elliptical or pear-shaped cylinders as the latter particles are more stable mechanically because of horizontal alignment by the base. One question which remains unresolved is how far the alignment propagates into the pile. In order to answer this question, the number of particles would need to be increased by an order of magnitude and this is left for a future study.

References

Aranson, I. S. & Tsimring, L. S. 2006 Patterns and collective behavior in granular media: theoretical concepts. *Rev. Mod. Phys.* **78**, 641–692. (doi:10.1103/RevModPhys.78.641)

Atman, A. P. F., Brunet, P., Geng, J., Reydellet, G., Claudin, P., Behringer, R. P. & Clément, E. 2005 From the stress response function (back) to the sand pile "dip". *Eur. Phys. J. E* **17**, 93–100. (doi:10.1140/epje/i2005-10002-2)

Bouchaud, J. P., Cates, M. E. & Claudin, P. 1995 Stress distribution in granular media and nonlinear wave equation. *J. Phys. I France* **5**, 639–656. (doi:10.1051/jp1:1995157)

Brockbank, B., Huntley, J. M. & Ball, R. C. 1997 Contact force distribution beneath a three-dimensional granular pile. *J. Phys. II France* **7**, 1521–1532. (doi:10.1051/jp2:1997200)

Buchalter, B. J. & Bradley, R. M. 1992 Orientational order in amorphous packings of ellipses. *J. Phys. A Math. Gen.* **25**, L1219–L1224. (doi:10.1088/0305-4470/25/21/003)

Cates, M. E., Wittmer, J. P., Bouchaud, J.-P. & Claudin, P. 1998 Development of stresses in cohesionless poured sand. *Phil. Trans. R. Soc. A* **356**, 2535–2560. (doi:10.1098/rsta.1998.0285)

Coppersmith, S. N., Liu, C.-h., Majumdar, S., Narayan, O. & Witten, T. A. 1996 Model for force fluctuations in bead packs. *Phys. Rev. E* **53**, 4673–4685. (doi:10.1103/PhysRevE.53.4673)

Corwin, E. I., Jaeger, H. M. & Nagel, S. R. 2005 Structural signature of jamming in granular media. *Nature* **435**, 1075–1078. (doi:10.1038/nature03698)

Dantu, P. 1968 Statistical study of intergranular forces in a powdery medium. *Geotechnique* **18**, 50.

de Gennes, P. G. 1999 Granular matter: a tentative view. *Rev. Mod. Phys.* **71**, S374–S382. (doi:10.1103/RevModPhys.71.S374)

Donev, A., Cisse, I., Sachs, D., Variano, E. A., Stillinger, F. H., Connelly, R., Torquato, S. & Chaikin, P. M. 2004 Improving the density of jammed disordered packings using ellipsoids. *Science* **303**, 990–993. (doi:10.1126/science.1093010)

Drescher, A. & De Josselin de Jong, G. 1972 Photoelastic verification of a mechanical model for the flow of a granular material. *J. Mech. Phys. Solids* **20**, 337–351. (doi:10.1016/0022-5096(72)90029-4)

Duran, J. 1999 *Sand, powders and grains: an introduction to the physics of granular materials.* New York, NY: Springer.

Edwards, S. F. & Oakeshott, R. B. S. 1989 The transmission of stress in an aggregate. *Physica D* **38**, 88–92. (doi:10.1016/0167-2789(89)90176-0)

Geng, J., Longhi, E., Behringer, R. P. & Howell, D. W. 2001 Memory in two-dimensional heap experiments. *Phys. Rev. E* **64**, 060301. (doi:10.1103/PhysRevE.64.060301)

Geng, J., Reydellet, G., Clément, E. & Behringer, R. P. 2003 Green's function measurements of force transmission in 2D granular materials. *Physica D* **182**, 274–303. (doi:10.1016/S0167-2789(03)00137-4)

Goldenberg, C. & Goldhirsch, I. 2005 Friction enhances elasticity in granular solids. *Nature* **435**, 188–191. (doi:10.1038/nature03497)

Hemmingsson, J., Herrmann, H. J. & Roux, S. 1997 Vectorial cellular automaton for the stress in granular media. *J. Phys. I France* **7**, 291–302. (doi:10.1051/jp1:1997146)

Howell, D., Behringer, R. P. & Veje, C. 1999 Stress fluctuations in a 2D granular Couette experiment: a continuous transition. *Phys. Rev. Lett.* **82**, 9241–9244. (doi:10.1103/PhysRevLett.82.5241)

Huntley, J. M. 1999 Force distribution in an inhomogeneous sandpile. *Eur. Phys. J. B* **8**, 389–397. (doi:10.1007/s100510050704)

Jaeger, H. M., Nagel, S. R. & Behringer, R. P. 1996 Granular solids, liquids, and gases. *Rev. Mod. Phys.* **68**, 1259–1273. (doi:10.1103/RevModPhys.68.1259)

Jotaki, T. & Moriyama, R. 1979 On the bottom pressure distribution of the bulk materials piled with the angle of repose. *J. Soc. Powder Technol. Jpn* **60**, 184–191.

Li, Y. J., Xu, Y. & Thornton, C. 2005 A comparison of discrete element simulations and experiments for 'sandpiles' composed of spherical particles. *Powder Technol.* **160**, 219–228. (doi:10.1016/j.powtec.2005.09.002)

Liffman, K., Chan, D. Y. C. & Hughes, B. D. 1994 On the stress depression under a sandpile. *Powder Technol.* **78**, 263–271. (doi:10.1016/0032-5910(93)02801-G)

Liffman, K., Nguyen, M., Metcalfe, G. & Cleary, P. 2001 Forces in piles of granular material: an analytic and 3D DEM study. *Gran. Matter* **3**, 165–176. (doi:10.1007/s100350100086)

Liu, C.-h., Nagel, S. R., Schecter, D. A., Coppersmith, S. N., Majumdar, S., Narayan, O. & Witten, T. 1995 Force fluctuations in beads packs. *Science* **269**, 513–515. (doi:10.1126/science.269.5223.513)

Luding, S. 1997 Stress distribution in static two-dimensional granular model media in the absence of friction. *Phys. Rev. E* **55**, 4720–4729. (doi:10.1103/PhysRevE.55.4720)

Luding, S. 2005 Granular media: information propagation. *Nature* **435**, 159–160. (doi:10.1038/435159a)

Lumay, G. & Vandewalle, N. 2004 Compaction of anisotropic granular materials: experiments and simulations. *Phys. Rev. E* **70**, 051314–051318. (doi:10.1103/PhysRevE.70.051314)

Majmudar, T. S. & Behringer, R. P. 2005 Contact force measurements and stress-induced anisotropy in granular materials. *Nature* **435**, 1079–1082. (doi:10.1038/nature03805)

Matuttis, H. G. 1998 Simulation of the pressure distribution under a two-dimensional heap of polygonal particles. *Grand. Matter* **1**, 83–91. (doi:10.1007/s100350050013)

Matuttis, H. G., Luding, S. & Herrmann, H. J. 2000 Discrete element simulations of dense packings and heaps made of spherical and non-spherical particles. *Powder Technol.* **109**, 278–292. (doi:10.1016/S0032-5910(99)00243-0)

Nielsen, J. 1998 Pressures from flowing granular solids in silos. *Phil. Trans. R. Soc. A* **356**, 2667–2684. (doi:10.1098/rsta.1998.0292)

Nouguier-Lehonn, C., Cambou, B. & Vincens, E. 2003 Influence of particle shape and angularity on the behaviour of granular materials: a numerical analysis. *Int. J. Numer. Anal. Meth. Geomech.* **27**, 1207–1226. (doi:10.1002/nag.314)

O'Hern, C. S., Langer, S. A., Liu, A. J. & Nagel, S. R. 2001 Force distributions near jamming and glass transition. *Phys. Rev. Lett.* **86**, 111–114. (doi:10.1103/PhysRevLett.86.111)

Ostojic, S., Somfar, E. & Nienhuis, B. 2006 Scale invariance and universality of force networks in static granular matter. *Nature* **439**, 828–830. (doi:10.1038/nature04549)

Savage, S. B. 1998 Modelling and granular material boundary value problems. In *Proc. Physics of Dry Granular Media, Cargese, France, 15–26 September 1997* (eds H. J. Herrmann, J.-P. Hovi & S. Luding), pp. 25–96. Dordrecht, The Netherlands: NATO Advanced Study Institute/Kluwer.

Smid, J. & Novosad, J. 1981 Pressure distribution under heaped bulk solids. *Ind. Chem. Eng. Symp.* **63**, D3/V/1–D3/V/12.

Stokely, K., Diacou, A. & Franklin Scott, V. 2003 Two-dimensional packing in prolate granular materials. *Phys. Rev. E.* **67**, 051302. (doi:10.1103/PhysRevE.67.051302)

Sugden, M. B. 1980 Effect of initial density on flow patterns in circular flat bottomed silos. In *Proc. Int. Conf. on Design of Silos for Strength and Flow, University of Lancaster, 11–28 September.*

Terzaghi, K. 1943 *Theoretical soil mechanics.* New York, NY: Wiley.

Vanel, L., Howell, D. W., Clark, D., Behringer, R. P. & Clément, E. 1999 Memories in sand: experimental tests of construction history on stress distributions under sandpiles. *Phys. Rev. E* **60**, R5040–R5043. (doi:10.1103/PhysRevE.60.R5040)

Veje, C., Howell, D. & Behringer, R. P. 1999 Kinematics of a two-dimensional granular Couette experiment at the transition to shearing. *Phys. Rev. E* **59**, 739–745. (doi:10.1103/PhysRevE.59.739)

Wittmer, J., Claudin, P., Cates, M. E. & Bouchaud, J. P. 1996 An explanation for the central stress minimum in sand piles. *Nature* **382**, 336–338. ([doi:10.1038/382336a0](doi:10.1038/382336a0))

Xu, N., Blawzdziewicz, J. & O'Hern, C. S. 2005 Random close packing revisited: ways to pack frictionless disks. *Phys. Rev. E* **71**, 061306. (doi:10.1103/PhysRevE.71.061306)

Zhong, Z., Ooi, J. Y. & Rotter, J. M. 2001 The sensitivity of silo flow and wall stresses to filling method. *Eng. Struct.* **23**, 756–767. ([doi:10.1016/S0141-0296(00)00099-7](doi:10.1016/S0141-0296(00)00099-7))

Zhou, J., Long, S., Wang, Q. & Dinsmore, A. D. 2006 Measurement of forces inside a three-dimensional pile of frictionless droplets. *Science* **312**, 1631–1633. (doi:10.1126/science.1125151)

Zuriguel, I., Maza, D., Pugnaloni, L. A., Pastor, J. M. & Garcimartín, A. 2005 Jamming during the discharge of granular matter from a silo. *Phys. Rev. E* **71**, 051303. (doi:10.1103/PhysRevE.71.051303)

Zuriguel, I., Mullin, T. & Rotter, J. M. 2007 The effect of particle shape on the stress dip under a sandpile. *Phys. Rev. Lett.* **98**, 028001. (doi:10.1103/PhysRevLett.98.028001)